Connecting experimental degradation kinetics to theoretical models for photocatalytic reactors: The influence of mass transport limitations

Nicole A.B. Timmerhuis, Jeffery A. Wood, Rob G.H. Lammertink *

Soft Matter, Fluidics and Interfaces, University of Twente, MESA+ Institute for Nanotechnology, P.O. Box 217, 7500 AE Enschede, the Netherlands

HIGHLIGHTS

- Mass transfer limitations are studied in wall-coated (photo)catalytic microreactors.
- Bisphenol A degradation is measured over TiO$_2$ for different light intensities.
- Excluding mass transfer can lead to underestimating the wall reaction rate.
- A literature study shows the effect of mass transfer on the apparent reaction rate

GRAPHICAL ABSTRACT
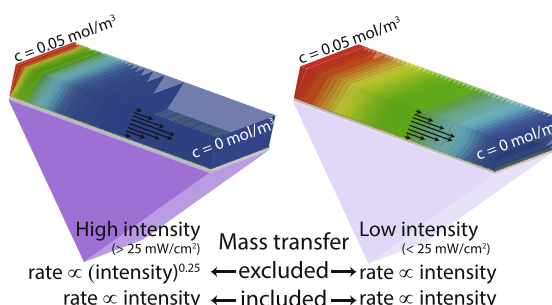
ABSTRACT

Catalytic microreactors offer great opportunities to measure reaction kinetics, and parameters influencing the reaction. Although microreactors are quite useful for characterizing catalysts, it is important to understand the relative contributions of mass transport and intrinsic kinetics to the apparent reaction rate. In this paper, we demonstrate the importance of accounting for mass transport limitations in the photocatalytic degradation of Bisphenol A over titanium dioxide. Using analytical scaling laws available from literature and numerical simulations, we provide guidelines for the use of microreactors in characterizing (photo)catalysts. These guidelines identify the mass transport limited regime, or the reaction rate limited regime. The photocatalytic degradation of Bisphenol A was found to be mass transport limited at high light intensities (photon fluxes of above 25 mW/cm^2). Neglecting the influence of mass transfer limitations in fitting kinetic data resulted in the exponent of reaction rate (β) with respect to light intensity to be $\beta \sim 0.25$, while including these effects gave an exponent directly proportional to the light intensity ($\beta \sim 1$). These findings stress the importance of a correct inclusion of mass transport limitations. A simple analysis of the transverse Péclet number and second Damköhler number, to quantify the transport and reaction rates, is presented for our laminar flow reactor to illustrate the different limiting regimes.

© 2021 The Authors. Published by Elsevier Ltd. This is an open access article under the CC BY license (http://creativecommons.org/licenses/by/4.0/).

1. Introduction

The state-of-art photoreactor is either a fixed-bed or slurry batch reactor (Herrmann, 2005) however, there is an increasing interest in microreactors. The reactor choice mainly depends on the research objective, for which Plutschack et al. (2017) made a

decision chart. A continuous flow (micro)reactor provides the advantage of precise control over process parameters. Catalytic microreactors are continuous flow reactors with the catalyst either as a fixed bed, in a micromonolith, or coated on the wall of the microreactor (Rossetti, 2018). In the last 20 years, a growing number of articles was published in this field, as shown in Fig. 1.

The reaction rate in photocatalysis is typically obtained from conversion experiments which are assessed by kinetic models (Herrmann, 2005; Visan and Lammertink, 2020). The most fre-
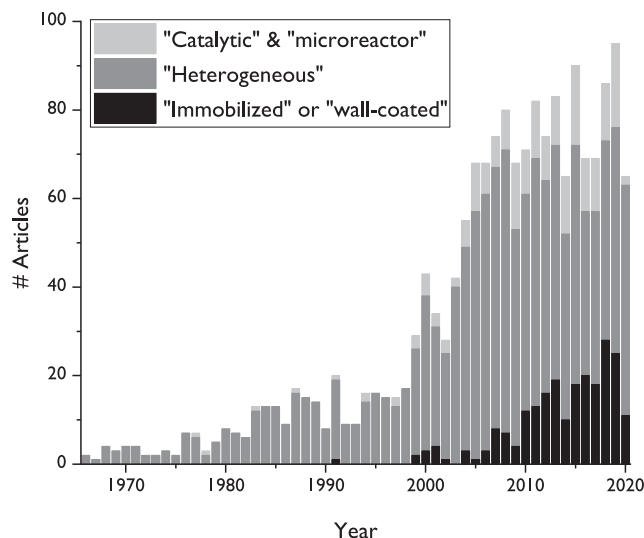

Fig. 1. Amount of articles published according to Scopus, accessed on 12th October 2020.

quently used model is the one-dimensional plug flow model, where all mass transfer is neglected which makes it straightforward and simple to use. On the other hand, Sherwood correlations provide information about mass transfer, and exist for different geometries with constant concentration or flux at the surface (Balakotaiah and West, 2002). Mass transfer can be included via more complex models, usually two or three-dimensional models which are solved numerically. Numerical methods are useful to extract more complex kinetic parameters, including more complex mass transfer, and when additional parameters influence the system, like photon flux for photocatalysis or temperature fluctuations.

Another common kinetic model is the Langmuir-Hinshelwood model in photocatalysis, which simplifies for low inlet concentration to a first-order reaction model (Herrmann, 2005) resulting in the one-dimensional plug flow model. This model describes the reaction kinetics limited regime as it does not include mass transfer. Including mass transfer and possible mass transport limitations leads to more complex expressions. Solbrig and Gidaspow (1967) derived a semi-analytical solution of a one-side coated rectangular catalytic microreactor, and Lopes et al. (2011) derived an analytical solution for symmetric, circular and rectangular, wall-coated microreactors. These models take advection and diffusion into account and are suitable for a quick assessment of the wall-coated catalyst.

Catalytic microreactors are dominated by advection, diffusion, and a reaction, which all have their own characteristic time scale (Squires et al., 2008). Advection is controlled by the flow velocity, with characteristic time scale $t_{adv} = L/u$, where L is the length of the reactor, and u the superficial velocity. Diffusion is generally a slow transport mechanism with a characteristic time scale $t_{diff} = l^2/D$, where l is the typical length (L or H, depending on the considered direction of diffusion), and D diffusion coefficient (Kirby, 2010). Consider a microreactor of $L \sim 10$mm, $H \sim 10\mu$m, $D \sim 5 \cdot 10^{-10}$ m^2/s, and $u \sim 10$mm/s, resulting in the time scales $t_{adv} \sim 1$s, $t_{diff,L} \sim 2 \cdot 10^{11}$s, and $t_{diff,H} \sim 0.2$s. Diffusion over the length of the channel is slow, but over the height of the channel it is in the same order of magnitude as advection.

The last important time scale comes from the reaction either in bulk or at the surface. For the bulk reaction $t_{bulkreaction} = k_{bulk}^{-1}$, where k_{bulk} is the bulk reaction rate, or for the surface reaction,

$t_{surfacereaction} = (k''a)^{-1}$, where k'' is the surface reaction rate and a the catalytic specific area. The bulk reaction rate is a time scale [s], whereas the surface reaction rate is a velocity [m/s]. These three time scales determine whether the reactor is reaction rate limited or mass transfer limited (Lopes et al., 2011).

It is crucial in order to properly assess the reaction kinetics that measurements are conducted in regimes where this information is accessible. To illustrate this point, articles from Fig. 1 are analysed if they contained wall-coated catalytic microreactors with first-order kinetics. The analysis uses the different time scales, $t_{advection}, t_{diffusion},$ and $t_{reaction}$ to determine the rate limiting regime.

We consider experimentally and theoretically a wall-coated photocatalytic microreactor to study the influence of mass transfer in interpreting reaction kinetics. The photocatalyst titanium dioxide (TiO$_2$) is chosen due to its rate dependency on the incident photon flux, as the reaction rate increases with increasing photon flux (Herrmann, 2005). The degradation of Bisphenol A (BPA) is considered as a model reaction, as this molecule has large consequences for aquatic life and can be completely mineralized by TiO$_2$ (Ohko, 2001).

In this article, one- and two-dimensional mathematical models are described to calculate the experimental reaction rate constant with and without considering mass transfer limitations. Secondly, the degradation of BPA over TiO$_2$ is experimentally determined for different photon fluxes. From there on, dimensionless numbers from the two dimensional model are used to identify different limiting regimes. Lastly, an extensive number of literature on experiments using catalytic wall coated microreactors are analysed and placed in the different limiting regimes. We provide an analysis which allows for rapid determination of the corresponding regime, as well as guidelines to design experiments for accurate intrinsic reaction constant evaluation.

2. Experimental

2.1. Microreactor fabrication

Our photocatalytic microreactor was fabricated in the MESA+ Nanolab cleanroom. We started with a wet thermally oxidized silicon wafer, with a silica layer of 1 μm. Photolithography with a positive photoresist (Olin Oir 907-17) was used to define the main channel patterns. Deep reactive ion etching was used to first etch the silica layer and secondly the main channel. Before the powder blasting, the channel was protected via spray coating photoresist (AZ4999) and adding a protection foil (Harke i-HC). Negative photoresist (SU8) was used create the mask on the back side, to powder blast the inlet and outlet of the channel. Afterwards, the photoresist and foil were stripped and remaining silica were removed with 1% BHF (buffered hydrogen fluoride).

Secondly, a MEMpax wafer was lithographically structured with a positive photoresist (Olin Oir 907-17) layer followed by reactive sputtering of oxidized titanium, according to Rafieian et al. (2015) at an oxygen pressure of 10^{-3} mbar for 90 minutes to create a layer of about 200 nm. After the sputtering, the photoresist layer was removed and lifts off the TiO$_2$, leaving only TiO$_2$ at the location of the main channels.

The silicon and MEMpax wafer were bonded together via anodic bonding and diced into reactors of 30x15 mm. Lastly, the TiO$_2$ layer was annealed in an oven at 500°C for two hours with a heating and cooling rate of 2 °C/min, resulting in a dense anatase TiO$_2$ layer. The TiO$_2$ layer was analysed with X-Ray Diffraction (XRD) to confirm the anatase crystalline structure, and with ellipsometry to determine the thickness. The rectangular reactor is 50 μm deep, 500 μm wide and 18 cm long, with a specific area of $9 \cdot 10^{-5}$ m^2.

2.2. Photocatalytic experiments

The microreactors were placed in a home-made reactor holder, of similar design to Visan and Lammertink (2020). The holder was made from aluminum, chosen for high thermal conductivity. The temperature was kept constant at 25°C with a Peltier element, QC-17-1.0-2.5MS, controlled by TEC software from Meerstetter Engineering and a PT100 temperature sensor. A Harvard PhD Ultra Syringe pump was used with a 5 mL Hamilton 1005 TLL gas tight glass syringe with PEEK tubing to and from the reactor. The TiO_2 was regenerated before each set of experiments using 30 w/w% hydrogen peroxide (ordered from Sigma Aldrich) and UV light for 30 minutes. After the regeneration, a higher activity of the photocatalyst was found so the catalyst is first stabilized for 1.5 hours before the start of the experiments. The Thorlabs SOLIS 365C was used as monochromatic UV source with a wavelength of 365nm, controlled by a DC2200 high power LED driver. The photon flux was measured for different currents by a Thorlabs PM100A power meter with S120VC sensor. The UV-LED illuminates the microreactor from below, through the MEMpax-side, on the TiO_2-layer inside the channel. The UV-LED has a warm-up time of 20 minutes for light intensities of above 50 mW/cm^2.

The degradation of BPA (purchased at Sigma Aldrich, $\geqslant 99\%$) was determined for different residence times and photon fluxes, with a constant inlet concentration of 50 mmol/m^3. The aqueous BPA solution was saturated with pure oxygen prior to the start of the experiments. The residence time was varied between 10 and 120s, with a photon flux between 1 and 250 mW/cm^2. Each experiment was performed in triplicate (N=3).

Degradation was determined by measuring the outlet concentration. Samples were collected after steady state was achieved and analyzed by a ThermoFisher Ultimate 3000 HPLC using a C18 column (Thermo Scientific Acclaim RSLC 120) with a water/acetonitrile and 0.1% phosphoric acid eluent. BPA concentration was determined in the HPLC via UV/Vis detection at 225nm.

3. Mathematical description

A mathematical description of the mass transport is essential to determine the surface reaction rate of the wall coated catalyst. Two models are considered, the most commonly used one-dimensional plug-flow model which neglects mass transport and the two-dimensional numerical model which includes mass transport by means of advection and diffusion. The one-dimensional model is easily solved analytically, whilst the two-dimensional model is typically solved numerically, although asymptotic solutions derived by Solbrig and Gidaspow (1967) are available. In the Supplementary Information, cases are provided for both top and bottom walls coated with catalyst, as well as for circular channels. These models are symmetric with respect to the middle of the channel, which alters the mathematical model slightly, and asymptotic analytical solutions were derived by Lopes et al. (2011).

3.1. One-dimensional model

The one-dimensional model (1D-model) is applicable in the absence of mass transfer limitations, as the reaction kinetics are limiting the conversion. This is known as the ideal plug-flow model, defined in Eq. 1 for a first-order reaction (Visan and Lammertink, 2020).

$$\frac{c}{c_0} = \exp(-k_{\text{bulk}}t) \tag{1}$$

where c is the outlet concentration [mol/m^3], c_0 the inlet concentration [mol/m^3], k_{bulk} the bulk reaction rate constant [s^{-1}], and t the residence time [s]. The bulk reaction rate constant relates to the

surface reaction rate constant for dense layers by $k'' = k_{\text{bulk}}/a$, where k'' is the surface reaction rate constant [m/s] and a the specific area of the catalyst [m^2/m^3].

3.2. Two-dimensional model

The two-dimensional model (2D-model) takes the following into account; advection, diffusion, and a first-order reaction at the wall. This is schematically shown in Fig. 2. The validity and limitations of this model are discussed first, followed by the governing equations and boundary conditions. The system is made non-dimensional to enable a general approach and to compare different time scales.

The motion of fluid is described by the Navier-Stokes equations. When the width is much larger than the height, the influence of the side walls can be neglected (Squires et al., 2008) and the fluid flow reduces to a two-dimensional velocity profile. Advection only occurs in the x-direction, whilst diffusion occurs in both the x- and y-direction, also called axial and transverse diffusion. This is described in the following equation

$$u(y)\frac{\partial c}{\partial x} = D\left(\frac{\partial^2 c}{\partial x^2} + \frac{\partial^2 c}{\partial y^2}\right) \tag{2}$$

where $u(y)$ is the height dependent velocity profile, c the molar concentration [mol/m^3], and D the diffusion coefficient [m^2/s].

The Reynolds number, which balances viscous forces over inertia, was between 0.08 and 0.9 in this system indicating laminar flow as expected (Squires and Quake, 2005). Hagen-Poisseuille flow is applicable with a parabolic velocity distribution

$$u(y) = 6\langle u\rangle\left(\frac{y}{H} - \left(\frac{y}{H}\right)^2\right) \tag{3}$$

where u is the velocity [m/s], $\langle u\rangle$ the average velocity, and H the channel height [m] (Bird et al., 2007).

Axial diffusion can be neglected when the axial diffusion time scale (L^2/D) is much larger than the residence time in the channel (Lopes et al., 2011), which is determined by the axial Péclet number.

$$Pe_{ax} = \frac{\langle u\rangle L}{D} \tag{4}$$

Axial diffusion can be neglected when $Pe_{ax} \gg 1$. The Péclet number in the experiments conducted ranged between $4.8 \cdot 10^5$ and $5.5 \cdot 10^6$, therefore axial diffusion was neglected.

The governing equation for the system presented in Fig. 2 then becomes

$$6\langle u\rangle\left(\frac{y}{H} - \left(\frac{y}{H}\right)^2\right)\frac{\partial c}{\partial x} = D\frac{\partial^2 c}{\partial y^2} \tag{5}$$
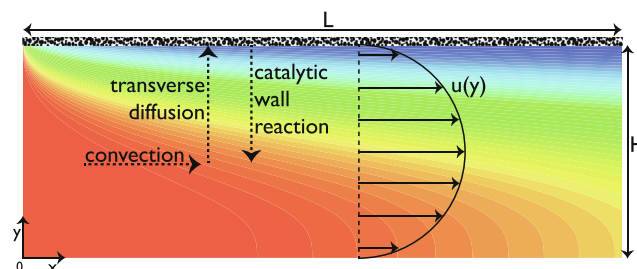

Fig. 2. Schematic of the model boundaries in Cartesian coordinates (x, y), with a laminar velocity flow profile. A concentration profile is given in color, where red is high concentration and blue is low concentration.

which is solved with the following boundary conditions. At first, the inlet concentration is set at c_0 and at the outlet as an open boundary condition, defined as zero normal gradient. Secondly, material cannot exit at the bottom wall, so there is no flux ($y = 0$), described by

$$\left.\frac{\partial c}{\partial y}\right|_{y=0} = 0 \tag{6}$$

Lastly, the catalytic wall at $y = H$ is described by a first-order reaction.

$$D\left.\frac{\partial c}{\partial y}\right|_{y=H} = -k''\eta c \tag{7}$$

where k'' is the surface reaction rate and η the internal effectiveness factor. The internal effectiveness factor is important for porous catalysts, as it describes the diffusion limitation into the catalytic pores. Additionally, porous photocatalysts can dependent on the light intensity, as the photon flux varies over the thickness of the catalyst layer. Both effects have been previously described by Visan et al. (2014). Here, the internal effectiveness factor is 1 as a dense photocatalyst is used.

3.3. Non-dimensional analysis

The model described above is made non-dimensional for easy comparison between articles and experiments, and furthermore illustrates the origin of the dimensionless transverse Péclet and second Damköhler numbers. The parameters are re-scaled as $\tilde{c} = c/c_0, \tilde{x} = x/L$, and $\tilde{y} = y/H$. The governing equation then becomes

$$6(\tilde{y} - \tilde{y}^2)Pe_H\frac{\partial\tilde{c}}{\partial\tilde{x}} = \frac{\partial^2\tilde{c}}{\partial\tilde{y}^2} \tag{8}$$

where Pe_H is the transverse Péclet number which is defined as

$$Pe_H = \frac{\langle u\rangle H^2}{LD} \tag{9}$$

The transverse Péclet number scales the transverse diffusion rate with the axial advection rate. Small Pe_H represents dominant transverse diffusion and for large Pe_H the advection dominates. Globally there are two different regimes which can be distinguished by the transverse Péclet number. The first one, the Graetz regime, is when transverse diffusion dominates the advective rate ($Pe_H \leqslant 1$). In the second regime, the Lévêque regime, the advective rate is dominant over the transverse diffusion rate ($Pe_H \gg 1$).

The boundary conditions are made dimensionless, similar to the governing equations. The inlet concentration becomes $\tilde{c} = 1$. Secondly, the no flux boundary condition at $\tilde{y} = 0$ becomes

$$\left.\frac{\partial\tilde{c}}{\partial\tilde{y}}\right|_{\tilde{y}=0} = 0 \tag{10}$$

Lastly, the first-order reaction at the catalytic wall at $\tilde{y} = 1$ becomes

$$\left.\frac{\partial\tilde{c}}{\partial\tilde{y}}\right|_{\tilde{y}=1} = -Da_{II}\tilde{c} \tag{11}$$

where Da_{II} is the second Damköhler number and defined as

$$Da_{II} = \frac{k''\eta H}{D} \tag{12}$$

The second Damköhler number relates the first-order reaction rate at the wall with the transverse diffusion rate (Squires et al., 2008). The diffusion rate dominates for $Da_{II} \ll 1$ and the reaction rate for $Da_{II} \gg 1$.

Additionally, a dimensionless concentration gradient, the mass transfer coefficient, can be defined to distinguish mass transfer

limitations (Lopes et al., 2011). It is defined as the concentration variance over the average concentration at a specific location x in the channel.

$$\theta(x) = \frac{\langle c\rangle(x) - c(x, 1)}{\langle c\rangle(x)} \tag{13}$$

where $\langle c\rangle(x)$ is the height averaged concentration, and $c(x, 1)$ the concentration at the catalytic wall. When mass transfer is much faster than the reaction rate, the concentration at the wall is approximately the average concentration over the height ($\langle c\rangle(x) \approx c(1, x)$), thus $\theta \approx 0$. The mass transfer limited regime is reached when the reaction is very fast so the concentration at the wall is approximately zero, $c(1, x) \approx 0$, and $\theta \approx 1$. As a rule of thumb, the system is in the kinetic limited regime when $\theta < 0.05$ and mass transfer controlled regime when $\theta > 0.95$.

The governing equation with the boundary conditions are solved numerically with the PDEPE-solver, with 500 grid points, in MATLAB v. 2019B. The experimental outlet concentrations vs. residence times were fit to the model in a least-squares sense to estimate the surface reaction rate constant (k''), with a function tolerance of 10^{-9} for the least squares fit.

4. Results and discussion

4.1. Degradation of Bisphenol A

The degradation of Bisphenol A (BPA) is measured for four different residence times in triplicate at each photon flux. The degradation of BPA is estimated using first-order reaction kinetics, as the inlet concentration is low (50 mmol/m³) and adsorption is not the rate-limiting step in this system (Herrmann, 2005). The light intensity was varied between 1 and 250 mW/cm². The residence time is varied between 10 and 120 seconds, corresponding to transverse Péclet numbers from 0.04 to 0.42, implying that all experiments are performed in the Graetz regime with a fully developed concentration profile.

Fig. 3 shows the degradation of BPA as a function of the residence time for different light intensities. The highest light intensity (~250 mW/cm²) results in full conversion for just 42s residence time, while the conversion is around 20% for the lowest light intensity (~1 mW/cm²) at 115s residence time. The conversion increases with light intensity, on account of the increasing photon

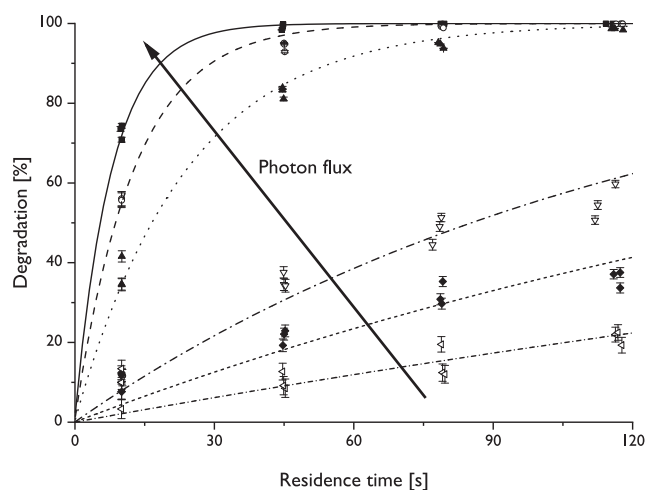**Fig. 3.** Degradation of BPA versus residence time for different light intensities: ~250 mW/cm² (–■–), ~100 mW/cm² (–⊖–), ~50 mW/cm² (··▲··), ~10 mW/cm² (–▽·–), ~5 mW/cm² (--◆--), and ~1 mW/cm² (--◀·-). The symbols are experimental results and the lines are fits based on the two-dimensional model.

flux. The more photons reach the photocatalyst, the more electron-hole pairs are formed and thus, the more organic compound is degraded. The lines in Fig. 3 represent the fitted data from the 2D-model. The resulting reaction rate constants are shown in Table 1, and plotted as a function of the light intensity in Fig. 4.

Firstly, the 1D-model is used to fit the experimental data to extract the bulk and surface reaction rate from Eq. (1). The results are shown in Table 1. As expected, the reaction rate increases with increasing light intensity. Fig. 4 shows a decreased slope for higher light intensities (above 25 mW/cm^2).

Secondly, the 2D-model data was fitted with one slope over the whole data regime, resulting in a slope of 0.82 ± 0.04. The slope for low and high light intensities were approximately equal to each other, therefore one slope over the whole range is representative for the data. The slope differs from 1 mainly because of the lowest and highest light intensity measurements. At the highest light intensity, the conversion was 100% for almost all residence times, meaning the reaction was limited solely by the amount of organic compound to degrade.

The surface reaction rate constant is related to the light intensity by $k'' = \alpha I^\beta$, where α depends on the specific reaction, and β determines the order (Herrmann, 2005). For many studies in batch reactors, it has been reported that the exponent β reduces at higher light intensities (above 25 mW/cm^2). This reduction is frequently attributed to the electron-hole pair recombination which becomes the rate limiting step in the process at high light intensities (Herrmann, 2005).

The 1D-model shows a similar trend with literature, with even a steeper decrease in slope for the higher light intensities. On the other hand, the 2D-model showed no decrease in slope for the higher light intensities compared to the lower light intensities, and the slope was approximately 1 over the entire range. This implies that the photoreaction rate was linearly proportional to the light intensity over the entire light intensity range studied. The only difference in the 1D- and 2D-model is the inclusion of mass transport for the 2D-model.

The resemblance between the theory, from a batch reactor, and the 1D-model arises from both approaches neglecting mass transport. Mass transport is not taken into account in a batch reactor, as it is an ideally stirred tank reactor (Herrmann, 2005). For very fast reactions, the concentration at the catalyst particle vanishes. This creates a boundary layer between the catalyst particle and liquid bulk, resulting in an apparent reaction rate with some mass transfer limitations. These mass transfer limitations are evidently reduced in batch studies carried out to date, as the slope decreased to 0.5 while even a larger decrease is observed when using the 1D-model. Here we show that the lower apparent reaction rate constant at higher photon fluxes can be the result of assessing reaction kinetics without including mass transport aspects, instead of the rate limiting step changing to the electron-hole pair recombination.

Fig. 4 shows the importance of including mass transport when determining the surface reaction rate. This is further explored in the next section, where general regimes are drafted indicating
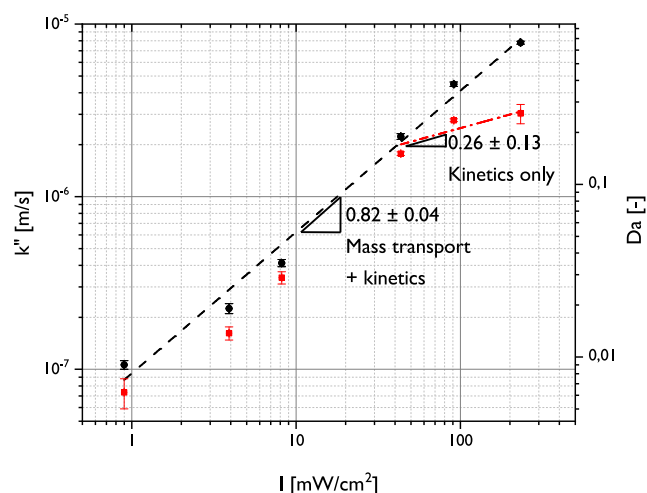

Fig. 4. Surface reaction rate constant and second Damköhler number as a function of the light intensity. The black points were fitted with the two-dimensional model (mass transport and kinetics) and the red points with the one-dimensional model (kinetics only).

the validity of the 1D-model and when to include mass transfer in deriving the reaction rate constant in a catalytic microreactor.

4.2. Influence of Mass Transfer

Several limiting regimes can be distinguished for the microreactors, based on the advection, diffusion and reaction time scales (Lopes et al., 2011). Firstly, mass transfer is limiting when diffusion time exceeds the residence time and the reaction is fast compared to diffusion ($t_{\text{diff,H}} \ll t_{\text{reaction}}$). Secondly, the kinetic limited regime occurs when the reaction is slow compared to mass transfer ($t_{\text{diff,H}} \gg t_{\text{reaction}}$). There is no substantial concentration gradient across the height of the reactor. Lastly, mass transfer and kinetics are both limiting when the typical time scales are similar ($t_{\text{diff,H}} \approx t_{\text{reaction}}$).

The 2D-model was made dimensionless, where three dimensionless numbers were derived. These three dimensionless numbers were the transverse Péclet number, Pe_H, the second Damköhler number, Da_{II}, and the dimensionless mass transfer coefficient, $\theta(x)$. Each dimensionless number distinguishes different operating regimes and together these provide a general analysis for mass transfer and kinetic limitations in a system.

The transverse Péclet number scales the transverse diffusion rate with the advection rate, and it determines the Graetz regime or the Lévêque regime. In the Graetz regime, the transverse diffusion is dominant over the advection ($Pe_H \leqslant 1$) and the concentration boundary layer is fully developed. In the Lévêque regime, advection is dominant over transverse diffusion ($Pe_H \gg 1$), creating a developing concentration boundary layer smaller than the channel height. The outlet concentration scales with $Pe_H^{1/3}$ in this developing concentration boundary layer (Solbrig and Gidaspow, 1967).

Table 1
The one-dimensional (1D) bulk and surface reaction rate, and the surface reaction rate and second Damköhler number from the two (2D) dimensional model, for each experimental photon flux.

I [m W/cm^2]	$k_{\text{bulk,1D}}$[1/s]	k_{1D} [μm/s]	k_{2D}[μm/s]	Da_{II}[-]
232 ± 0.5	0.0607 ± 0.0078	3.03 ± 0.39	7.80 ± 0.15	0.66 ± 0.01
91.1 ± 0.1	0.0554 ± 0.0011	2.77 ± 0.05	4.50 ± 0.13	0.38 ± 0.01
43.4 ± 0.1	0.0355 ± 0.0009	1.78 ± 0.04	2.23 ± 0.09	0.19 ± 0.007
8.17 ± 0.01	0.0068 ± 0.0006	0.34 ± 0.03	0.41 ± 0.02	0.035 ± 0.002
3.90 ± 0.01	0.0032 ± 0.0003	0.16 ± 0.01	0.22 ± 0.01	0.019 ± 0.001
0.899 ± 0.004	0.0015 ± 0.0003	0.07 ± 0.01	0.11 ± 0.01	0.009 ± 0.01

The second Damköhler number determines whether the transverse diffusion rate is limiting compared to the reaction rate. Transverse diffusion dominates when $Da_{II} \ll 1$ and the reaction rate dominates for $Da_{II} \gg 1$. Lastly, the mass transfer coefficient (θ) determines whether the system is mass transfer or reaction rate limited. The dimensionless mass transfer coefficient θ depends solely on the second Damköhler number in the Graetz regime. In the Lévêque regime it additionally scales to $Pe_H^{1/3}$ due to the developing concentration boundary layer (Solbrig and Gidaspow, 1967). The limiting regimes are graphically shown in Fig. 5a.

Fig. 5a shows the transverse Péclet number versus second Damköhler number. On the left side we have the Graetz regime with a fully developed concentration profile and on the right side the Lévêque regime with the developing concentration profile. Similarly, we can go from the bottom to the top by increasing the reaction rate. Previously, $\theta < 0.05$ was set as a rule of thumb for the reaction rate controlled region and $\theta > 0.95$ for the mass transfer controlled region (Lopes et al., 2011). Here it shows that for $Da_{II} < 0.1$ the system is reaction rate limited in the fully developed regime, and mass transfer limitations increase gradually with increasing second Damköhler numbers.

Fig. 5b shows different concentration profiles along the complete channel, for given transverse Péclet and second Damköhler numbers. Dark red represents the inlet concentration and dark blue represents zero concentration, with the catalytic wall at $y = 1$. The inlet is at $x = 0$ and outlet at $x = 1$. Concentration profiles [A]-[E] are conform with the letters in Fig. 5a.

Profiles [A] and [B] are both in the mass transfer controlled regime, where [A] has a fully developed concentration profile, meaning equal relative concentration distribution across the channel height at each x location, and [B] a developing concentration profile with a growing boundary layer. The reaction rate is very high for both so the concentration near the catalyst becomes zero in both profiles. Profile [A] is mass transfer limited due to low superficial velocity and profile [B] due to low transverse diffusion, so in both cases there is insufficient reactant supply towards the catalyst which results in mass transfer limitations.

Profile [C] is controlled equivalently by mass transfer and reaction rate, and located in the transfer region from developed to developing concentration profile. The developing concentration profile is most clearly shown here, as the concentration at the catalytic wall changes over the length of the channel compared to the average concentration. Also, the boundary layer is protruding towards the other wall but does not reach it, implying a still developing concentration profile. This case is both mass transfer and

reaction rate controlled, as the transverse diffusion rate and reaction at the wall are both limiting.

Profile [D] and [E] are both in the reaction rate controlled region, where [D] has a fully developed concentration profile and [E] a developing concentration profile. The transverse diffusion rate is ten times faster than the advective rate for [D], resulting in almost no concentration difference over the height of the channel. The conversion is thus determined by the reaction rate at the wall, and the average concentration variance over the length is the same as the concentration at the wall. Therefore, the region of profile [D], Graetz regime and low second Damköhler number, can also be described by the 1D-model, the plug flow model. Lastly, profile [E] has a slow reaction rate and high convective rate, resulting in a barely visible concentration boundary layer, so there is no significant conversion.

In the model, the transverse Péclet number and second Damköhler number determine the outlet concentration, and thus the conversion. Fig. 6 shows a surface graph of the conversion for the same Pe_H-Da_{II}-landscape as previously shown. Each Da_{II}-number ranges all conversions, dependent on the Pe_H-number. However, the conversion does not increase anymore with increasing Damköhler in the mass transfer limited regime ($Da_{II} > 35$ in the developed concentration region). This means that for one Pe_H-number a range of Da_{II}-numbers match for one conversion, thus the Da_{II}-number cannot be uniquely determined in that range.

The conversion of a compound is usually kept low to determine kinetic rate constants. The low conversion prevents mass transfer limitations as large concentration gradients are prevented in the reactor. However, for a microreactor it is possible to measure without mass transfer limitations also at high conversions, as can be seen in Fig. 6.

The degradation of BPA over TiO_2 was measured at transverse Péclet numbers of 0.04 till 0.42. The photon flux was varied, resulting in second Damköhler numbers from 0.01 till 0.66, so from the kinetic limited regime towards the mixed controlled regime. The significance of mass transfer limitations increases with increasing photon fluxes, above 25 mW/cm². When the same experimental data is treated with the 1D-model, a lower surface reaction rate constant is obtained, as was shown in Fig. 4.

Process design and optimization could benefit from the Pe_H-Da_{II}-graph with the limiting regimes. Industrial processes want the highest production rate for the lowest cost. Fig. 6 shows the conversion for all limiting regimes in the Pe_H-Da_{II}-graph. When the surface reaction rate, diffusion coefficient and optimal conversion are known, a micro-reactor can be designed with optimal
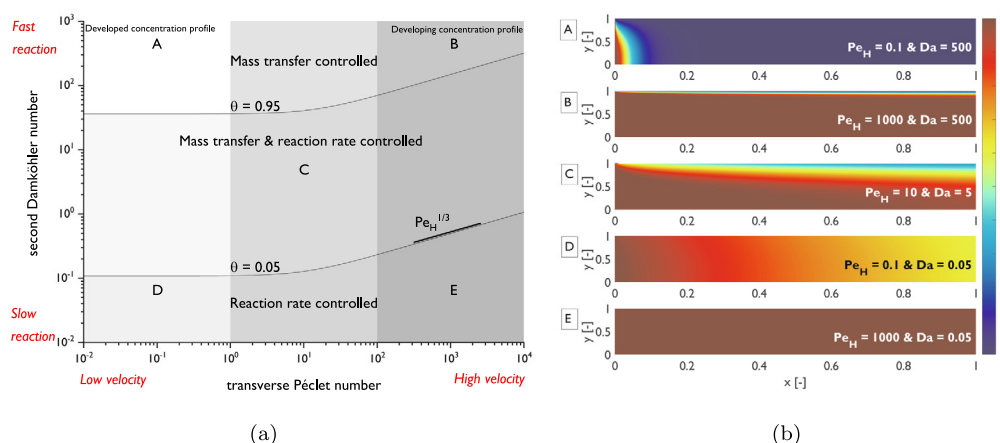

Fig. 5. Left; Combining the transverse Péclet number, second Damköhler number and mass transfer coefficient (for laminar flow) in a graph to show the limiting regimes. Right; Concentration profiles for different transverse Péclet and second Damköhler numbers.
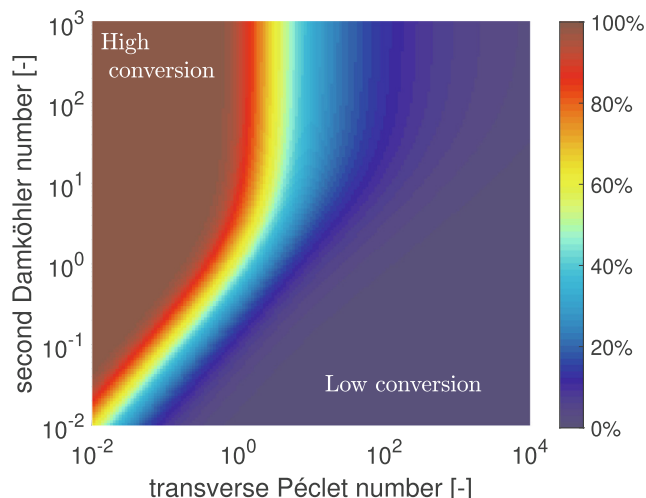
Fig. 6. The Pe_H–Da_{II}-graph with the conversion plotted as surface, where dark red is full conversion and dark blue is no conversion.

height, length, and superficial velocity. The process can then be scaled-up by matching the width and amount of channels to the desired production rate.

4.3. Comparison with literature

The articles found via the Scopus search in Fig. 1 were further selected for having a wall-coated catalyst with first-order reaction in either circular or rectangular channels, with laminar flow. The surface reaction rate, and second Damköhler number, were fitted with the 2D-model provided here for one-wall coated reactor or in the Supplementary Information for top and bottom wall coated reactors. The results are shown in Fig. 7.

Fig. 7 presents a variety of studies including zeolites and biological catalysts. Many studies operate in the Graetz regime ($Pe_H < 1$)

with kinetic limitations ($Da_{II} < 0.1$) and without significant mass transfer limitations (region [D] in Fig. 5a). Some studies which do operate with mass transfer limitations (towards region [C] and beyond) are discussed hereafter.

Nakamura et al. (2004) immobilized silica colloidal particles in circular channels with different diameters. The silica particles were functionalized with either photocatalyst or enzymes. The enzyme reactor operates very close to the $\theta = 0.05$ iso-curve and thus has some mass transfer limitations. The photocatalytic reactors operate close to the Léve~que-regime at $Da_{II} \approx 50$ for the TiO$_2$ and $Da_{II} \approx 5$ for the TiO$_2$/SiO$_2$ catalyst, resulting in a high mass transfer coefficients ($\theta \approx 0.96$ & 0.43 respectively). Here, the combination of a fast reaction (methylene blue to leucomethylene blue) and high surface area results in severe mass transfer limitations.

Li et al. (2018) immobilized palladium nanoparticles in UiO-66-NH$_2$-films to study the conversion of 4-nitrophenol to 4-aminophenol, with control over the Pd-loading. The second Damköhler number is fitted at around 5, with the mass transfer coefficient of 0.7 for the lower Pd-loading, indicating both reaction and mass transfer limitations. The higher Pd-loading case could not be fitted as the conversion was always around 100% and there is insufficient information to extract rate kinetics. Mass transfer limitations occur due to the relatively large inner diameter and high palladium loading.

Li et al. (2018) proposed a photocatalytic microreactor with catalyst at top and bottom wall with increased specific surface area (dual film reactor), and compared it to a one-wall coated photocatalytic reactor with conventional 1D-model to extract a bulk reaction rate, per residence time. The conversion, and their k_{bulk}-value, was found to be higher for the dual film reactor compared to the single film reactor and they attribute the better performance to better mass transfer. Here, we considered single and dual catalyst wall models to extract the surface reaction rate constants. The Da_{II}-number was fitted for the single and dual film at 1.8 and 0.7 respectively, with a surface reaction rate constant of $5 \cdot 10^{-6}$ m/s and $4 \cdot 10^{-6}$ m/s respectively. Although the dual film has a higher conversion, the single film has a faster surface reaction rate, likely
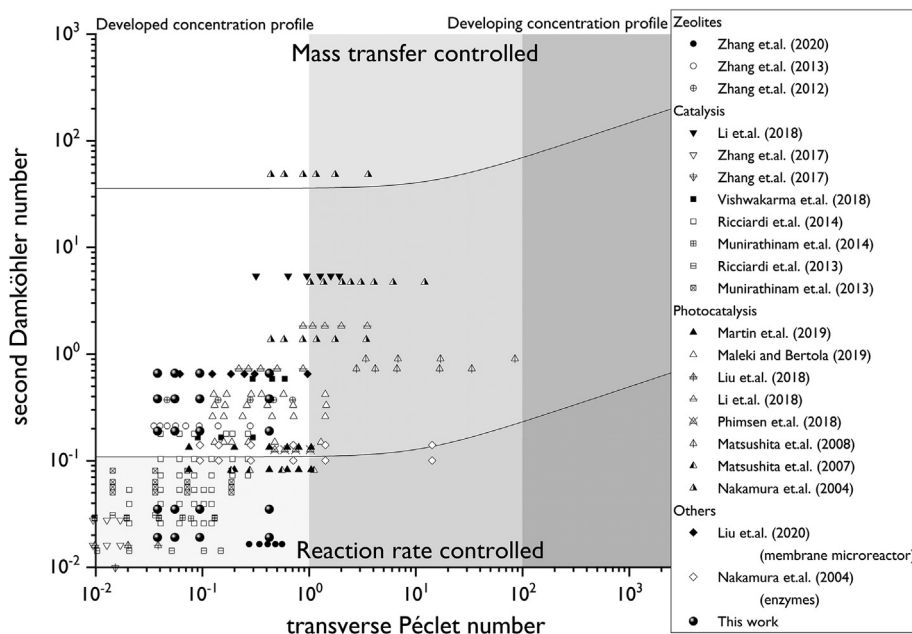

Fig. 7. Transverse Péclet versus second Damköhler number fitted for the available literature (Zhang et al. (2020),Zhang et al. (2013), Zhang et al. (2012),Li et al. (2018), Zhang et al. (2017),Zhang et al. (2017), Vishwakarma et al. (2018),Ricciardi et al. (2014), Munirathinam et al. (2014),Ricciardi et al. (2013), Munirathinam et al. (2013),Martin et al. (2019), Maleki and Bertola (2019),Liu et al. (2018), Li et al. (2018),Phimsen et al. (2017), Matsushita et al. (2008),Matsushita et al. (2007), Nakamura et al. (2004),Liu et al. (2020)).

caused by the improved illumination. The efficiency of the single film reactor would surpass the dual film reactor by also using a dual film.

Matsushita et al. (2008) studied the photocatalytic degradation and reduction of organic compounds in a micromilled microreactor with a rough surface. The rough surface increases the specific area of the catalyst, and the experiments were performed close to the Lévêque regime, resulting in low conversions. The results were fitted with a second Damköhler number around 1, implying some mass transfer limitations. The mass transfer limitations would decreased by increasing the residence time and decreasing the channel height. With that, the compound has more time to reach the surface and has to overcome a shorter distance.

The remaining articles shown in Fig. 7 can roughly be divided in two categories; articles which operate in the kinetic limited regime (Ricciardi et al., 2014; Zhang et al., 2020; Zhang et al., 2017; Zhang et al., 2017; Munirathinam et al., 2014; Ricciardi et al., 2013; Munirathinam et al., 2013; Martin et al., 2019; Liu et al., 2018; Phimsen et al., 2017; Matsushita et al., 2007) and articles which operate in the mixed limited regime(Vishwakarma et al., 2018; Zhang et al., 2012; Liu et al., 2020; Maleki and Bertola, 2019; Zhang et al., 2013; Ricciardi et al., 2014). The articles operating in the mixed limited regime ($\theta > 0.05$) have some mass transfer limitations and should take these into account when determining the surface reaction rate constant. The studies performed in the region without mass transfer limitations can use the simple 1D plug-flow model to calculate the reaction rate constant.

5. Conclusion

The degradation of BPA over TiO_2 has been studied for different photon fluxes. For high photon fluxes, above 25 mW/cm^2, mass transfer limitations become apparent. The appearance of mass transport limitations can result in an underestimation of the surface reaction rate constant.

The analysis with transverse Péclet number, second Damköhler number, and mass transfer coefficient proved efficient in distinguishing in which limiting regime a system operates. Different studies were analysed on mass transfer limitations, mainly in the field of photocatalysis, although it also proved useful for other catalysis studies. Mass transfer limitation can easily occur in catalytic microreactors, and can be overcome by changing the superficial velocity, reactor geometry, or reaction rate (in case of photocatalysis). The Pe_H-Da_{II}-graph can provide clear insight in the operation of a microreactor and assist in optimizing the design.

Declaration of Competing Interest

The authors declare that they have no known competing financial interests or personal relationships that could have appeared to influence the work reported in this paper.

Acknowledgement

Appendix A. Titanium dioxide characterization and experimental setup

The sputtered TiO_2 layer is analysed with SEM, XRD and ellipsometry. The results can be compared to the original published articles by Rafieian et al. (2015).

The SEM pictures show a smooth TiO_2 surface after the sputtering, and some cracks in the surface after annealing, which is similar to Rafieian et al. (2015).

The XRD was measured to confirm an anatase crystalline TiO_2-layer, which was measured at an angle of 20-30° with an increment of 0.002 and 10 rpm. Anatase TiO_2 would show a peak at 25°, while rutile would show a peak around 27°. From the XRD and SEM can be concluded that an anatase crystalline TiO_2-layer is formed.(see Fig. S1)

Ellipsometry is used to measure the thickness of the layer and the extinction coefficient. The extinction coefficient gives information about the absorbance of light by the layer. The thickness of the layer is approximately 300nm, and the extinction coefficient is plotted in Fig. S2b. The extinction coefficient increases with lower wavelengths, which was expected as TiO_2 absorbs light with energies higher than 365nm.

The reactor holder is shown in Fig. S3a, where the green tubing is the inlet and the brown one is the outlet. The Peltier element is secured with an aluminium plate, with on top a static cooler. Fig. S3b shows the holder from the bottom, where the channel can be seen. The opening is made so the UV-light can reach the TiO_2 from the bottom side.

Appendix B. Mathematical description for catalyst on both walls

Here, the mathematical description is given for systems with catalyst on both walls, top and bottom. We consider both polar and Cartesian coordinates, as these correspond to the most common cases for a microreactor (circular cross-sections or thin rectangular slabs). The main difference between the one wall coated and two wall coated models is that the two wall coated model has symmetry in the middle of the channel, schematically shown for the half channel height or radius in Fig. S4.

The geometry is either a rectangular or circular channel. The rectangular channel is described in Cartesian coordinates (x, y) and assumes homogeneous catalyst coating on the wall, so the model is symmetrical from the middle of the channel and the typical height is the half the channel height ($a = H/2$). The circular channel is described in polar coordinates (r, z) and is also symmetrical in the middle of the channel, so the typical height is the radius of the channel ($a = R$).

The governing equation describes the advection and transverse diffusion for the rectangular channel as following

$$u(y)\frac{\partial c}{\partial x} = D\frac{\partial^2 c}{\partial y^2} \tag{S1}$$

where c is the concentration in $[mol/m^3]$. The circular channel is different in coordinate system, so the governing equation then becomes

$$u(r)\frac{\partial c}{\partial z} = D\left(\frac{1}{r}\frac{\partial}{\partial r}\left(r\frac{\partial c}{\partial r}\right)\right) \tag{S2}$$

The velocity profiles are again dependent on the height

$$u(y) = \frac{3}{2}\langle u\rangle(y)\left(1 - \left(\frac{y}{a}\right)^2\right) \tag{S3}$$

for a rectangular channel where $a = H/2$

$$u(r) = 2\langle u\rangle(r)\left(1 - \left(\frac{r}{a}\right)^2\right) \tag{S4}$$

for a circular channel, where $a = R$.

The boundary conditions for a rectangular channel are similar to the one-wall coated model, only the no-flux boundary condition at $y = 0$ is now replaced with a symmetry boundary condition. For the circular channel, the inlet concentration is c_0 and there is also
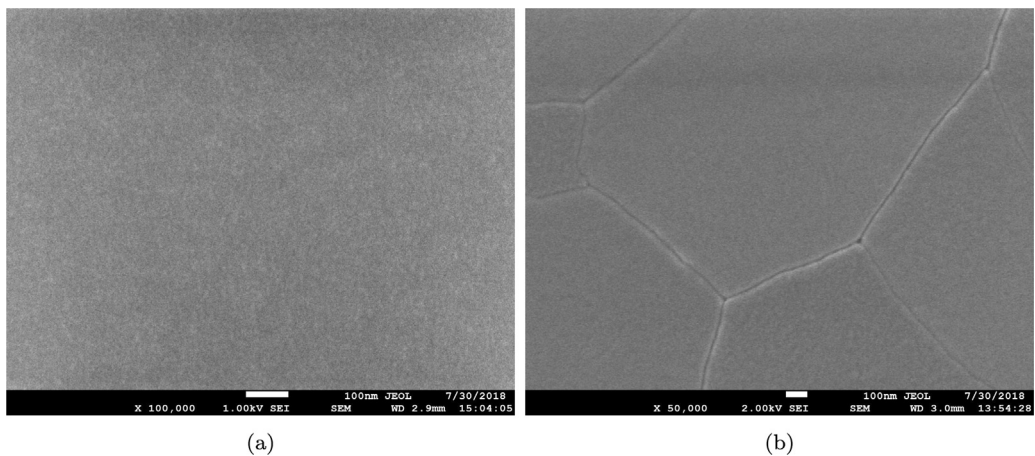
Fig. S1. SEM pictures of the TiO₂ surface taken before (left) and after (right) annealing.

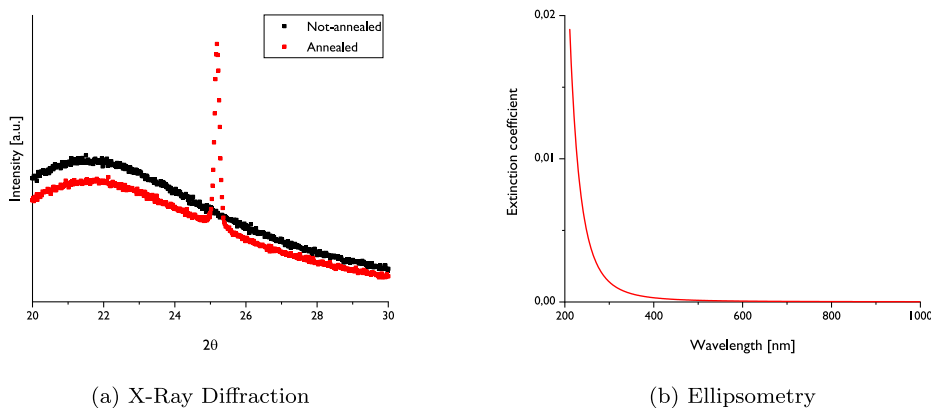(a) X-Ray Diffraction

(b) Ellipsometry

Fig. S2. X-Ray Diffraction results (left) before and after annealing the TiO₂-layer and extinction coefficient (right) as a function of the wavelength, measured with Ellipsometry.
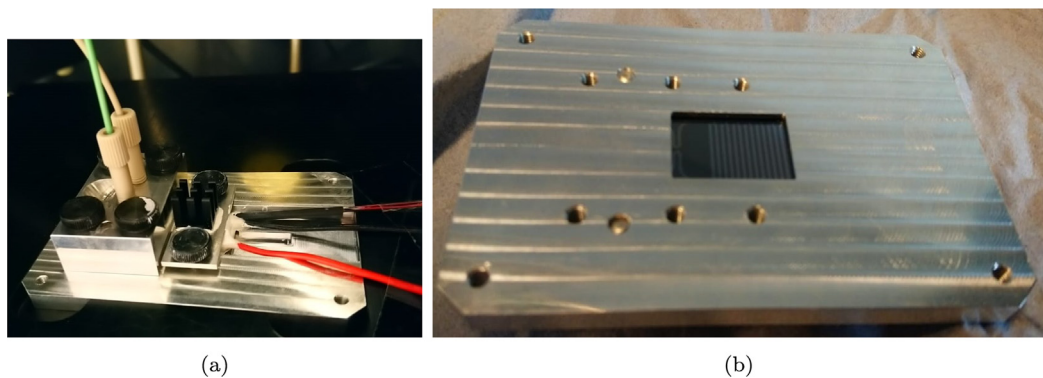

Fig. S3. Reactor holder from the top (left) and bottom (right).

symmetry in the middle of the channel. The catalytic wall is described by

$$D \frac{\partial c}{\partial r}\bigg|_{r=a} = -k'' \eta c \tag{S5}$$

The model is made non-dimensional again. The same scaling is used for the rectangular channel, $\tilde{c} = c/c_0, \tilde{x} = x/L, \tilde{y} = y/a$, and for the circular channel $\tilde{z} = z/L$ and $\tilde{r} = r/a$. The governing equations then become

$$\frac{3}{2}(1 - \tilde{y}^2) Pe_H \frac{\partial \tilde{c}}{\partial \tilde{x}} = \frac{\partial^2 \tilde{c}}{\partial \tilde{y}^2} \tag{S6a}$$

$$2(1 - \tilde{r}^2) Pe_H \frac{\partial \tilde{c}}{\partial \tilde{z}} = \frac{1}{\tilde{r}} \frac{\partial}{\partial \tilde{r}} \left(\tilde{r} \frac{\partial \tilde{c}}{\partial \tilde{r}} \right) \tag{S6b}$$

for the rectangular and circular channel respectively. The transverse Péclet number is the same as for the one-wall coated rectangular channel
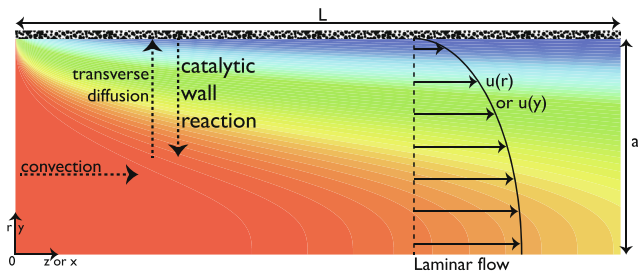
Fig. S4. Schematic of the model boundaries with a laminar velocity flow profile in Cartesian coordinates (x, y) for a rectangular channel and polar coordinates (r, z). A concentration profile is given in color, where red is the begin concentration and blue is zero concentration.

$$Pe_H = \frac{\langle u \rangle a^2}{LD} \tag{S7}$$

The boundary conditions are also made dimensionless. The inlet concentration becomes $\tilde{c} = 1$, there is still symmetry in the middle of the channel and the first-order reaction at the wall for rectangular channel is

$$\left. \frac{\partial \tilde{c}}{\partial \tilde{y}} \right|_{\tilde{y}=1} = -\frac{k'' \eta a}{D} \tilde{c} = -Da_{II} \tilde{c} \tag{S8}$$

and for a circular channel

$$\left. \frac{\partial \tilde{c}}{\partial \tilde{r}} \right|_{\tilde{r}=1} = -\frac{k'' \eta a}{D} \tilde{c} = -Da_{II} \tilde{c} \tag{S9}$$

where Da_{II} is the second Damköhler number and, again, defined as

$$Da_{II} = \frac{k'' \eta a}{D} \tag{S10}$$

This set of equations represents a rectangular channel with catalyst coated on both walls, and a circular channel with catalyst coated on the wall. The equations were made dimensionless, so it can be used more global and different systems can be compared fairly to each other. An analytical solution to these is provided by Lopes et al. (2011).

References

Balakotaiah, V., West, D.H., 2002. Shape normalization and analysis of the mass transfer controlled regime in catalytic monoliths. Chem. Eng. Sci. 57, 1269–1286. https://doi.org/10.1016/S0009-2509(02)00059-3.

Bird, R., Stewart, W., Lightfoot, E., 2007. Transport Phenomena. John Wiley & Sons.

Herrmann, J.M., 2005. Heterogeneous photocatalysis: state of the art and present applications. Topics in Catalysis 34, 49–65. https://doi.org/10.1007/s11244-005-3788-2.

Kirby, B.J., 2010. Micro- and Nanoscale Fluid Mechanics. Cambridge University Press (CUP).

Li, J., Wu, F., Lin, L., Guo, Y., Liu, H., Zhang, X., 2018. Flow fabrication of a highly efficient Pd/UiO-66-NH2 film capillary microreactor for 4-nitrophenol reduction. Chem. Eng. J. 333, 146–152. https://doi.org/10.1016/j.cej.2017.09.154.

Li, L., Tang, D., Song, Y., Jiang, B., 2018. Dual-film optofluidic microreactor with enhanced light-harvesting for photocatalytic applications. Chem. Eng. J. 339, 71–77. https://doi.org/10.1016/j.cej.2018.01.074.

Liu, A.-L., Li, Z.-Q., Wu, Z.-Q., Xia, X.-H., 2018. Study on the photocatalytic reaction kinetics in a TiO2 nanoparticles coated microreactor integrated microfluidics device. Talanta 182, 544–548. https://doi.org/10.1016/j.talanta.2018.02.028.

Liu, M., Zhu, X., Liao, Q., Chen, R., Ye, D., Chen, G., 2020. Stacked Catalytic Membrane Microreactor for Nitrobenzene Hydrogenation. Ind. Eng. Chem. Res. 59, 9469–9477. https://doi.org/10.1021/acs.iecr.0c01234.

Lopes, J.P., Rodrigues, A.E., Cardoso, S.S.S., 2011. Approximate calculation of conversion with kinetic normalization for finite reaction rates in wall-coated microchannels. AIChE J. 57, 2870–2887. https://doi.org/10.1002/aic.12483.

Lopes, J.P., Cardoso, S.S.S., Rodrigues, A.E., 2011. Criteria for kinetic and mass transfer control in a microchannel reactor with an isothermal first-order wall reaction. Chem. Eng. J. 176–177, 3–13. https://doi.org/10.1016/j.cej.2011.05.088.

Maleki, H., Bertola, V., 2019. TiO2 Nanofilms on Polymeric Substrates for the Photocatalytic Degradation of Methylene Blue. ACS Applied Nano Materials 2, 7237–7244. https://doi.org/10.1021/acsanm.9b01723.

Martin, M.V., Alfano, O.M., Satuf, M.L., 2019. Cerium-doped TiO2 thin films: Assessment of radiation absorption properties and photocatalytic reaction efficiencies in a microreactor. Journal of Environmental Chemical Engineering 7, 103478. https://doi.org/10.1016/j.jece.2019.103478.

Matsushita, Y., Ohba, N., Kumada, S., Suzuki, T., Ichimura, T., 2007. Photocatalytic N-alkylation of benzylamine in microreactors. Catal. Commun. 8, 2194–2197. https://doi.org/10.1016/j.catcom.2007.04.033.

Matsushita, Y., Ohba, N., Kumada, S., Sakeda, K., Suzuki, T., Ichimura, T., 2008. Photocatalytic reactions in microreactors. Chem. Eng. J. 135, S303–S308. https://doi.org/10.1016/j.cej.2007.07.045.

Munirathinam, R., Ricciardi, R., Egberink, R.J.M., Huskens, J., Holtkamp, M., Wormeester, H., Karst, U., Verboom, W., 2013. Gallium-containing polymer brush film as efficient supported Lewis acid catalyst in a glass microreactor. Beilstein J. Org. Chem. 9, 1698–1704. https://doi.org/10.3762/bjoc.9.194.

Munirathinam, R., Huskens, J., Verboom, W., 2014. Piperazine-containing polymer brush layer as supported base catalyst in a glass microreactor. Journal of Flow Chemistry 4, 135–139. https://doi.org/10.1556/JFC-D-14-00020.

Nakamura, H., Li, X., Wang, H., Uehara, M., Miyazaki, M., Shimizu, H., Maeda, H., 2004. A simple method of self assembled nano-particles deposition on the micro-capillary inner walls and the reactor application for photo-catalytic and enzyme reactions. Chem. Eng. J. 101, 261–268. https://doi.org/10.1016/j.cej.2003.11.022.

Ohko, Y., Ando, I., Niwa, C., Tatsuma, T. Yamamura, T. Nakashima, T., Kubota, Y., Fujishima, A., 2001, Degradation of bisphenol A in water by TiO2 photocatalyst. Environmental Science and Technology 35, 2365–2368. https://doi.org/10.1021/es001757t.

Phimsen, S., Yamada, H., Tagawa, T., Kiatkittipong, W., Kiatkittipong, K., Laosiripojana, N., Assabumrungrat, S., 2017. Epoxidation of methyl oleate in a TiO2 coated-wall capillary microreactor. Chem. Eng. J. 314, 594–599. https://doi.org/10.1016/j.cej.2016.12.017.

Plutschack, M.B., Pieber, B., Gilmore, K., Seeberger, P.H., 2017. The Hitchhiker's Guide to Flow Chemistry. Chem. Rev. 117, 11796–11893. https://doi.org/10.1021/acs.chemrev.7b00183.

Rafieian, D., Driessen, R.T., Ogieglo, W., Lammertink, R.G.H., 2015. Intrinsic Photocatalytic Assessment of Reactively Sputtered TiO2 Films. ACS Applied Materials & Interfaces 7, 8727–8732. https://doi.org/10.1021/acsami.5b01047.

Ricciardi, R., Huskens, J., Verboom, W., 2013. Heterogeneous acid catalysis using a perfluorosulfonic acid monolayer-functionalized microreactor. Journal of Flow Chemistry 3, 127–131. https://doi.org/10.1556/JFC-D-13-00024.

Ricciardi, R., Munirathinam, R., Huskens, J., Verboom, W., 2014. Improved catalytic activity and stability using mixed sulfonic acid-and hydroxy-bearing polymer brushes in microreactors. ACS Applied Materials and Interfaces 6, 9386–9392. https://doi.org/10.1021/am5017717.

Rossetti, I., 2018. Continuous flow (micro-)reactors for heterogeneously catalyzed reactions: Main design and modelling issues. Catal. Today 308, 20–31. https://doi.org/10.1016/j.cattod.2017.09.040.

Solbrig, C.W., Gidaspow, D., 1967. Convective diffusion in a parallel plate duct with one catalytic wall - Laminar Flow - First order reaction part I - Analytical, The. Can. J. Chem. Eng. 45, 35–39. https://doi.org/10.1002/cjce.5450450109. http://doi.wiley.com/10.1002/cjce.5450450109.

Squires, T.M., Quake, S.R., 2005. Microfluidics: Fluid physics at the nanoliter scale. Rev. Mod. Phys. 77, 977–1026. https://doi.org/10.1103/RevModPhys.77.977.

Squires, T.M., Messinger, R.J., Manalis, S.R., 2008. Making it stick: Convection, reaction and diffusion in surface-based biosensors. Nat. Biotechnol. 26, 417–426. https://doi.org/10.1038/nbt1388.

Visan, A., Lammertink, R.G.H., 2020. Fructose dehydration to hydroxyl-methylfurfural in an immobilized catalytic microreactor. Journal of Flow Chemistry. https://doi.org/10.1007/s41981-020-00087-5.

Visan, A., Rafieian, D., Ogieglo, W., Lammertink, R.G.H., 2014. Modeling intrinsic kinetics in immobilized photocatalytic microreactors. Applied Catalysis B: Environmental 150–151, 93–100. https://doi.org/10.1016/j.apcatb.2013.12.003.

Vishwakarma, N.K., Hwang, Y.-H., Adiyala, P.R., Kim, D.-P., 2018. Flow-Assisted Switchable Catalysis of Metal Ions in a Microenvelope System Embedded with Core-Shell Polymers. ACS Applied Materials & Interfaces 10, 43104–43111. https://doi.org/10.1021/acsami.8b17926.

Zhang, G., Zhang, X., Lv, J., Liu, H., Qiu, J., Yeung, K.L., 2012. Zeolite capillary microreactor by flow synthesis method. Catal. Today 193, 221–225. https://doi.org/10.1016/j.cattod.2012.04.008.

Zhang, T., Zhang, X., Yan, X., Kong, L., Zhang, G., Liu, H., Qiu, J., Yeung, K.L., 2013. Synthesis of Fe3O4@ZIF-8 magnetic core–shell microspheres and their potential application in a capillary microreactor. Chem. Eng. J. 228, 398–404. https://doi.org/10.1016/j.cej.2013.05.020.

Zhang, L., Liu, Z., Wang, Y., Xie, R., Ju, X.-J., Wang, W., Lin, L.-G., Chu, L.-Y., 2017. Facile immobilization of Ag nanoparticles on microchannel walls in microreactors for catalytic applications. Chem. Eng. J. 309, 691–699. https://doi.org/10.1016/j.cej.2016.10.038.

Zhang, L., Liu, Z., Liu, L.-Y., Ju, X.-J., Wang, W., Xie, R., Chu, L.-Y., 2017. Novel Smart Microreactors Equipped with Responsive Catalytic Nanoparticles on Microchannels. ACS Applied Materials and Interfaces 9, 33137–33148. https://doi.org/10.1021/acsami.7b09939.

Zhang, G., Zhang, L., Wang, X., Chen, A., Zhang, Q., 2020. Microfluidic processing of hzsm-5 films in a capillary microreactor for the continuous acetalisation reaction of glycerol with acetone. Reaction Chemistry and Engineering 5, 539–546. https://doi.org/10.1039/c9re00450e, cited By 0.